

Origin of the transitions inversion in rare-earth vanadates

Xue-Jing Zhang,¹ Erik Koch,² and Eva Pavarini¹

¹Peter Grünberg Institute, Forschungszentrum Jülich, 52425 Jülich, Germany

²Jülich Supercomputing Centre, Forschungszentrum Jülich, 52425 Jülich, Germany
(Dated: November 26, 2024)

The surprising inversion of the orbital- and magnetic-order transition temperatures in the RVO_3 series with increasing the rare-earth radius makes the series unique among orbitally-ordered materials. Here, augmenting dynamical mean-field theory with a decomposition of the order parameter into irreducible tensors, we show that this anomalous behavior emerges from an unusual hierarchy of interactions. First, increasing the rare-earth radius, orbital physics comes to be controlled by xz - xz quadrupolar super-exchange rather than by lattice distortion. Next, for antiferromagnetic spin order, orbital super-exchange terms with different spin rank compete, so that the dipolar spin-spin interaction dominates. Eventually, G-type magnetic order (anti-ferro in all directions) can appear already *above* the orbital ordering transition, and C-type order (anti-ferro in the ab plane) right around it. The strict constraints we found explain why the inversion is rare, giving at the same time criteria to look for similar behavior in other materials.

Introduction. The interplay of the spin, orbital and lattice degrees of freedom in strongly-correlated transition-metal oxides results in a plethora of phenomena of puzzling complexity [1–3]. In recent years, heterostructuring, disorder and non-equilibrium techniques [4–6] have opened the path to discovering or engineering new phases. In this panorama, the series of t_{2g}^2 perovskites RVO_3 (where R is a rare-earth) is paradigmatic [7–27]. In fact, they exhibit a set of different phases, structural and electronic, whose onset depends on the rare-earth radius R_I . They are orthorhombic $GdFeO_3$ -type perovskites at high temperature and become monoclinic at a temperature T_S ; the orthorhombic phase is, however, either re-entrant at $T_S < T_S$ (small R_I), or coexists with the monoclinic phase in a large temperature window (e.g., for intermediate R_I) [12, 20]. Structural changes have been identified with changes in orbital ordering (OO).

The truly peculiar aspect of the phase diagram, however, is the reversal of the spin- and orbital-ordering transition with increasing R_I . For small R_I , an anti-ferro (AF) magnetic transition occurs at $T_N < T_S$, of C-type in the monoclinic and G-type in the orthorhombic phase [20–25]. Orbital fluctuations, however, are already suppressed in the high-temperature phase [28–30], i.e., OO itself arises at a temperature $T_{OO} > T_S$. This is the classic scenario for OO – in fact, in almost all known orbitally-ordered materials, from $LaMnO_3$ and $KCuF_3$ to rare-earth titanates, OO precedes spin ordering ($T_N < T_{OO}$). Yet, in RVO_3 systems, increasing R_I , magnetic and orbital transition approach each other ($T_N \rightarrow T_{OO}$), and eventually invert around Ce and La [25–27], a highly unusual behavior. The complex phase diagram of the rare-earth vanadates is believed to be the result of the interplay of lattice distortion, leading to a sizable intra- t_{2g} crystal-field (CF) splitting, and super-exchange (SE) effects of the Kugel’ and Khomskii (KK) type [31]. Indeed, we recently have identified $LaVO_3$ as an orbitally-ordered system of the KK kind [32]. What, however, controls the surprising inversion of the orbital- and magnetic-order transition with increasing R_I is not understood.

In this work we address and solve this problem. We show that the inversion is the result of an unusual balance of interactions. When R_I is small, lattice distortions suppress the most efficient orbital SE channels. This yields the “classical” picture [33–37] with the orbital state mostly controlled by the CF splitting and $T_N < T_{OO}$. Increasing R_I , however, reinforces xz - xz quadrupolar SE, which, eventually, controls orbital physics; yet, AF spin-spin interactions grow as well, while, at the same time, orbital SE terms of different spin rank compete. In the end, the energy balance tilts, leading to G-type AF magnetic ordering *preceding* OO. The resulting phase diagram is shown schematically in Fig. 1.

Model and Method. We adopt the local-density approximation+dynamical mean-field theory (LDA+DMFT) approach. First we perform local-density-approximation calculations using the full-potential linearized augmented plane-wave method as implemented in the WIEN2K code [38]. Next we construct Wannier functions spanning the t_{2g} bands using the maximal localization procedure

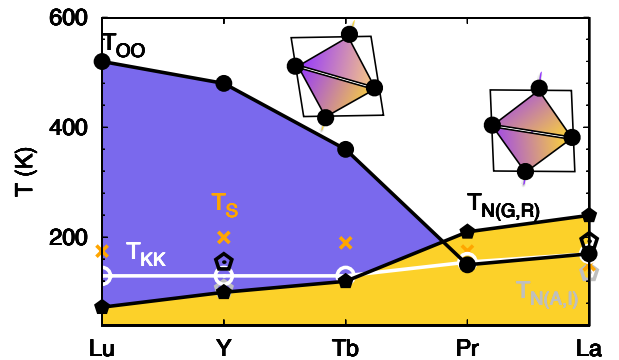


FIG. 1. Phase diagram. Filled black circles: orbital-ordering temperature T_{OO} . Empty white circles: Kugel-Khomskii transition temperature T_{KK} . Hexagons: magnetic transition temperature T_N ; G-type (black) and A-type (grey) AF. R : real structure. I : idealized case with no CF splitting. T_S : experimental structural transition (from [25]).

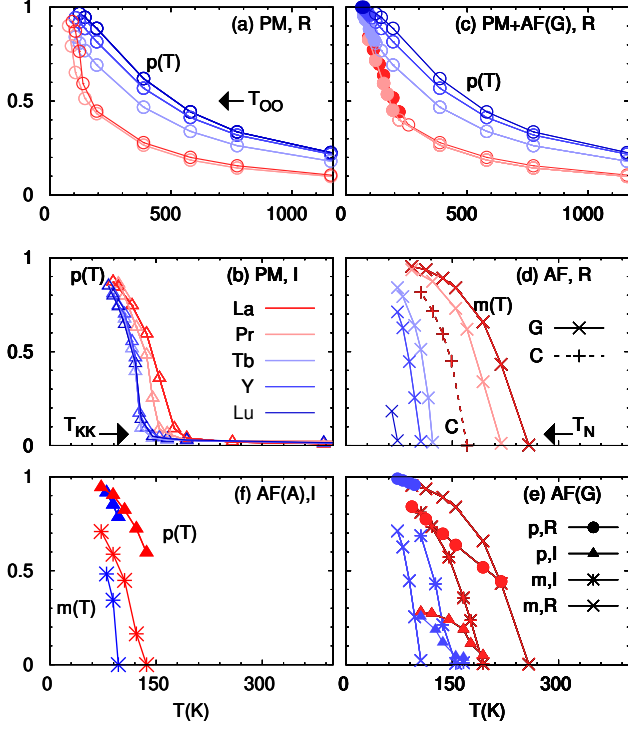


FIG. 2. LDA+DMFT results. Orbital and magnetic transitions in the RVO_3 series. Order parameters: $p(T)$ (orbital polarization) and $m(T)$ (magnetic moment). Open circles: $p(T)$, paramagnetic (PM) phase. Filled circles: $p(T)$, AF phase. I : idealized case with no CF splitting. R : experimental structure; T_{OO} : temperature yielding $p=0.5$. AF: antiferromagnetic of G-, C-, A-type.

[39, 40]. Finally, we build the associated Hubbard model

$$\begin{aligned} \hat{H} = & - \sum_{i i' \sigma} \sum_{m m'} t_{m m'}^{i, i'} c_{i m \sigma}^\dagger c_{i' m' \sigma} + U \sum_{i m} \hat{n}_{i m \uparrow} \hat{n}_{i m \downarrow} \\ & + \frac{1}{2} \sum_{i \sigma \sigma'} \sum_{m \neq m'} (U - 2J - J \delta_{\sigma, \sigma'}) \hat{n}_{i m \sigma} \hat{n}_{i m' \sigma'} \\ & - J \sum_{i m \neq m'} (c_{i m \uparrow}^\dagger c_{i m \downarrow}^\dagger c_{i m' \uparrow} c_{i m' \downarrow} + c_{i m \uparrow}^\dagger c_{i m \downarrow} c_{i m' \uparrow}^\dagger c_{i m' \downarrow}^\dagger). \end{aligned} \quad (1)$$

Here $t_{m m'}^{i, i'}$ is the hopping integral from orbital m on site i to orbital m' on site i' , and $\varepsilon_{m m'}^{i, i} = -t_{m m'}^{i, i}$ is the crystal-field matrix. The operator $c_{i m \sigma}^\dagger$ ($c_{i m \sigma}$) creates (annihilates) an electron with spin σ in Wannier state m at site i , and $n_{i m \sigma} = c_{i m \sigma}^\dagger c_{i m \sigma}$. The screened Coulomb parameters adopted are $U=5$ eV and $J=0.68$ eV, established values for this type of systems [29, 41, 42]. We solve this model using the dynamical mean-field theory. We adopt the generalized hybridization-expansion continuous-time quantum Monte Carlo method [43], in the implementation of Refs. 44–46, for the solution of the quantum impurity problem. We define the orbital polarization, the order parameter for OO, as $p(T) = (n_3 + n_2) / 2 - n_1$, where n_i are the occupations of the natural orbitals, ordered such

that $n_{i+1} \geq n_i$. The magnetization is $m(T) = (n_\uparrow - n_\downarrow) / 2$, where $n_{i\sigma} = \sum_m n_{i m \sigma}$. In the t_{2g}^2 configuration, in the atomic limit, the ground multiplet is 3P , a spin and orbital triplet. The orbital triplet states can be written as $|\bar{m}_3\rangle = |m_1 m_2\rangle$, where $m_1 \neq m_2$ are the occupied orbitals and \bar{m}_3 the empty orbital, with $m_i \in \text{span}(xy, xz, yz)$ [30]. Using this notation, the hole orbital at site i is

$$|\theta, \phi\rangle_\alpha^i = \sin \theta \cos \phi |xz\rangle + \cos \theta |xy\rangle + \sin \theta \sin \phi |yz\rangle. \quad (2)$$

In the $GdFeO_3$ -type structure, there are four (equivalent) V sites in the unit cell. The reference site is $i=1$, and for simplicity we set $|\theta, \phi\rangle_\alpha^1 = |\theta, \phi\rangle_\alpha$; the hole-orbitals for the remaining sites are constructed by symmetry [47]. The label α in Eq. (2) specifies how the state is obtained: $|\theta, \phi\rangle_{OO}$, from LDA+DMFT calculations for the experimental structure; $|\theta, \phi\rangle_{KK}$, from LDA+DMFT calculations for an idealized structure with no CF splitting; $|\theta, \phi\rangle_M$, maximizing the SE total energy gain (see next section). Finally, the highest energy CF state is $|\theta, \phi\rangle_{CF}$.

Super-exchange Hamiltonian. The crucial element of the puzzle is the materials-specific SE Hamiltonian [31]. Recently we introduced a systematic approach to build it from (1) via irreducible-tensor decomposition [30, 35]. This yields $\hat{H}_{SE} = \frac{1}{2} \sum_{ij} \hat{H}_{SE}^{i,j}$, with

$$\hat{H}_{SE}^{i,j} = \sum_{qq'} \sum_{\nu\nu'} \sum_{rr'} \sum_{\mu\mu'} \hat{\tau}_i^{r\mu; q\nu} D_{r\mu, r'\mu'}^{ij; q\nu} \hat{\tau}_j^{r'\mu'; q\nu} \quad (3)$$

where $r=0, 1, 2$ is the orbital rank (monopole, dipole, quadrupole) with components $\mu = -r, \dots, r$, and $q = 0, 1$ (monopole, dipole) is the spin rank with components $\nu = -q, \dots, q$. It is convenient to split Eq. (3) as

$$\hat{H}_{SE}^{i,j} = \hat{H}_{C_{ij}} + \hat{H}_{O_i O_j} + \hat{H}_{S_i S_j} + \hat{H}_{S_i S_j O_i O_j}. \quad (4)$$

The first term, $\hat{H}_{C_{ij}}$, obtained by setting $r=r'=q=q'=0$, in the absence of charge ordering, is a constant, independent on orbital and spin state; here we take it as the energy zero. The second term, $\hat{H}_{O_i O_j}$, obtained by setting $q=0$ and $r+r' \neq 0$, describes the interaction between orbital pseudospins, independent of the magnetic state. The third term ($r=r'=0$ and $q \neq 0$) describes a pure spin-spin interaction, independent of the orbital state. Finally the last term, obtained for $r+r' \neq 0, q=1$, is $\hat{H}_{S_i S_j O_i O_j}$, and describes the entangling of spins and orbitals. The analytic expressions of the tensor elements $D_{r\mu, r'\mu'}^{ij; q\nu}$ can be found in Ref. 30. They depend on U, J and the hopping integrals; the latter are listed in the Supplemental Material [48]. From Eq. (3) we calculate $\Delta E(\theta, \phi)$, the SE energy for a given spin and orbital ordering; minimizing it with respect to the angles yields $|\theta, \phi\rangle_M$. Finally, in order to unravel the complexity of the emergent ordering, we resort to a novel scheme: we decompose the order parameter itself into its irreducible components, $p_q = \sum_{r>0\mu} a_{r\mu; q0} \langle \hat{\tau}_i^{r\mu; q0} \rangle$; the orbital polarization is $p=p_0$, while $m = \langle \hat{\tau}_i^{00; 10} \rangle$. Last, the expectation value of an operator for a specific hole orbital [49] is $\langle \hat{\tau}_i^{r;\mu} \rangle_\alpha = \langle \theta, \phi | \hat{\tau}_i^{r;\mu; q\nu} | \theta, \phi \rangle_\alpha$.

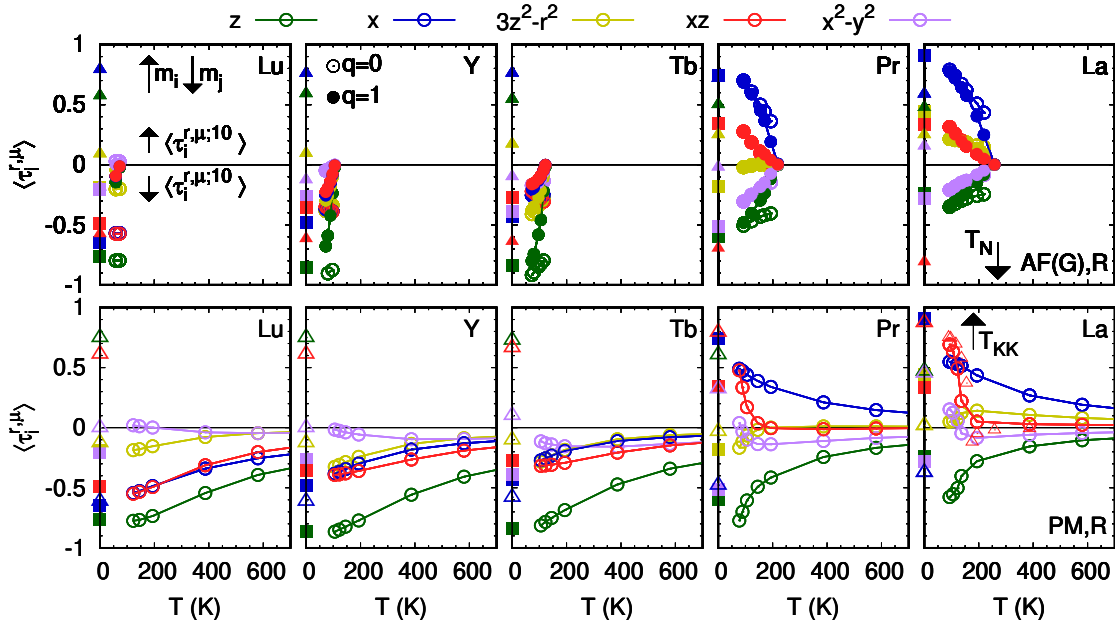


FIG. 4. Irreducible components of the order parameter, $\langle \hat{\tau}_i^{r,\mu;q\nu} \rangle$, normalized to the maximum value they can reach [48]. $T=0$ axis: $\langle \theta, \phi | \hat{\tau}_i^{r,\mu;q\nu} | \theta, \phi \rangle_\alpha$ for $\alpha=M$ (triangles) and $\alpha=CF$ (filled square). Bottom: PM phase (empty symbols). Top: AF (G) (filled symbols). The magnetization is $m_i = m > 0$ at site i (Fig. 2) and $m_j = -m$ at a neighboring site.

dipolar spin-spin term, (s, s) . The latter, taken alone, depends little on OO or the CF. We find that such a term is AF in all directions, Fig. 3; in the AF (G) phase, it is also the dominant magnetic interaction. Its strength increases with R_I , in particular along \mathbf{c} , i.e., it is weaker for small R_I ; in the ideal case with no CF, it is just strong enough to make T_N slightly larger than T_{KK} for all R_I , see Fig. 2, panel (e). It is only when we switch on the CF splitting, that we obtain the inversion of T_N and T_{KK} with increasing R_I .

This surprising effect is a consequence of the spin-orbital coupling via the $\hat{H}_{S_i S_j O_i O_j}$ SE term. Fig. 4, top panel, shows that the $q=1$ and $q=0$ operators have similar expectation value below T_N . All the $q=1$ expectation values, however, alternate sign for two AF neighboring sites (i, j) : thus, for $r+r' > 1$, the $q=1$ and $q=0$ contributions tend to cancel each other, see Fig. 3, AF(G) panel, for the limit of full magnetization. The channels influencing T_N are then mostly (s, μ) terms with spin rank $q=1$ and $\mu = x, z$. For small R_I , in the presence of CF, the latter are ferromagnetically aligned ($m_j \langle \hat{\tau}_i^{r,\mu} \rangle > 0$ for all neighbors j , see Fig. 4); this leads to magnetic frustration, reducing T_N ; for large R_I , instead, the alignment is antiferro in three channels, increasing T_N . This is why, for the real structures, $T_N > T_{KK} < T_{OO}$ for large R_I but $T_N < T_{KK} \sim T_{OO}$ when R_I is small.

Let us now consider other possible AF magnetic structures: C-type, with ferro (F) order along \mathbf{c} , and A-type, with F order in the \mathbf{ab} plane (the latter is not found experimentally for these systems). In both the A and C structures, for at least one bond the (s, s) component of the spin-spin interaction is frustrated. This, taken alone,

reduces T_N . The F stacking, either along \mathbf{c} or in the plane, is stabilized by terms with orbital rank $r+r' > 0$, hence by OO, however. For La, Fig. 2 shows that indeed $T_N \lesssim T_{KK}$ for C-type magnetic order. Entering the monoclinic phase, *ceteris paribus*, does not change this conclusion: the (s, s) magnetic term remains in fact essentially the same; C-type spin order is assisted by the CF splitting [50]. Finally, in the A phase, there is no magnetic order without OO for the systems considered, since the (s, s) spin-spin orbital monopolar interaction alone gives an energy loss, see Fig. 2, panel (f).

Conclusion. In conclusion, using a new analysis scheme based onto the decomposition of the order parameter into its irreducible components, we explained the origin of the inversion of T_N and T_{OO} with increasing R_I in vanadates. Our results clarify why the T_N - T_{KK} inversion is rare: in most orbitally ordered systems the onset of orbital ordering is determined by lattice distortions, i.e., T_{OO} is controlled by the CF splitting, rather than SE. The inversion instead requires that two conditions are simultaneously verified: (i) that $T_{OO} \sim T_{KK}$, and (ii) that nonetheless the magnetic structure is determined by dipolar interactions with orbital rank $r=0$. This indicates that small R_I systems could be manipulated to satisfy these conditions and provides criteria to look for similar behavior in other materials. Finally, the approach used in this work should prove powerful for understanding other classes of problems, such as the nature of octupolar order in materials with strong spin-orbit coupling.

We would like to acknowledge computational time on JURECA as well as on JUWELS; the latter was used in particular for code development.

- [1] D.I. Khomskii, *Transition Metal Compounds*, Cambridge University Press (2014).
- [2] Y. Tokura and N. Nagaosa, *Science* **288**, 462-468 (2000).
- [3] E. Dagotto, *Science* **309**, 257-262 (2005).
- [4] H. Y. Hwang, Y. Iwasa, M. Kawasaki, B. Keimer, N. Nagaosa, and Y. Tokura, *Nat. Mat.* **11**, 103-113 (2012).
- [5] J. Yan, A. Kumar, M. Chi, M. Brahlek, T. Z. Ward, and M.A. McGuire, *Phys. Rev. Mat.* **8**, 024404 (2024).
- [6] A. S. Disa, J. Curtis, M. Fechner, A. Liu, A. von Hoegen, M. Först, T. F. Nova, P. Narang, A. Maljuk, A. V. Boris, B. Keimer, and A. Cavalleri, *Nature* **617**, 73-78 (2023).
- [7] P. Horsch, A. M. Oleś, L. F. Feiner and G. Khaliullin, *Phys. Rev. Lett.* **100**, 167205 (2008).
- [8] M. J. Martínez-Lope, J. A. Alonso, M. Retuerto, and M. T. Fernández-Díaz, *Inorg. Chem.* **47**, 2634 (2008).
- [9] J.-S. Zhou, Y. Ren, J.-Q. Yan, J.F. Mitchell, and J. B. Goodenough, *Phys. Rev. Lett.* **100**, 046401 (2008).
- [10] Y. Ren, A. A. Nugroho, A. A. Menovsky, J. Stremfper, U. Rütt, F. Iga, T. Takabatake and C. W. Kimball, *Phys. Rev. B* **67**, 014107 (2003).
- [11] J.-Q. Yan, J.-S. Zhou, and J. B. Goodenough, *Phys. Rev. Lett.* **93**, 235901 (2004).
- [12] M. H. Sage, G. R. Blake, G. J. Nieuwenhuys, and T. T. M. Palstra, *Phys. Rev. Lett.* **96**, 036401 (2006).
- [13] P. N. Shanbhag, F. Fauth, and A. Sundaresan, *Phys. Rev. B* **108** 134115 (2023).
- [14] M. Nasir, I. Kim, Ki. Lee, S. Kim, K. Hyoung Lee, and H. Jung Park *Phys. Chem. Chem. Phys.* **25**, 3942 (2023).
- [15] H. Meley, M. Tran, J. Teyssier, J. A. Krieger, T. Prokscha, A. Suter, Z. Salman, M. Viret, D. van der Marel, and S. Gariglio, *Phys. Rev. B* **103**, 125112 (2021).
- [16] J.-Q. Yan, W. Tian, H. B. Cao, S. Chi, F. Ye, A. Llobet, A. Puretzky, Q. Chen, J. Ma, Y. Ren, J.-G. Cheng, J.-S. Zhou, M. A. McGuire, and R. J. McQueeney, *Phys. Rev. B* **100** 184423 (2019).
- [17] E. Benckiser, L. Fels, G. Ghiringhelli, M. Moretti Sala, T. Schmitt, J. Schlappa, V. N. Strocov, N. Mufti, G. R. Blake, A. A. Nugroho, T. T. M. Palstra, M. W. Haverkort, K. Wohlfeld, and M. Grüninger, *Phys. Rev. B*, **88** 205115 (2013).
- [18] F. Novelli, D. Fausti, J. Reul, F. Cilento, P. H. M. van Loosdrecht, A. A. Nugroho, T. T. M. Palstra, M. Grüninger, and F. Parmigiani, *Phys. Rev. B* **86**, 165135 (2012).
- [19] K. Ruotsalainen, M. Gatti, J.M. Ablett, F. Yakhou-Harris, J.-P. Rueff, A. David, W. Prellier, and A. Nicolaou, *Phys. Rev. B* **103**, 235158 (2021).
- [20] M. H. Sage, G. R. Blake, C. Marquina, and T. T. M. Palstra, *Phys. Rev. B* **76**, 195102 (2007).
- [21] G. R. Blake, T. T. M. Palstra, Y. Ren, A. A. Nugroho, and A. A. Menovsky, *Phys. Rev. Lett.* **87**, 245501 (2001).
- [22] M. Reehuis, C. Ulrich, K. Prokeš, S. Matáš, J. Fujioka, S. Miyasaka, Y. Tokura, and B. Keimer, *Phys. Rev. B* **83**, 064404 (2011).
- [23] R. Saha, F. Fauth, V. Caignaert, and A. Sundaresan, *Phys. Rev. B* **95**, 184107 (2017).
- [24] M. Reehuis, C. Ulrich, P. Pattison, M. Miyasaka, Y. Tokura, and B. Keimer, *Eur. Phys. J. B* **64**, 27-34 (2008).
- [25] S. Miyasaka, Y. Okimoto, M. Iwama, and Y. Tokura, *Phys. Rev. B* **68**, 100406(R) (2003).
- [26] J.-S. Zhou, J. B. Goodenough, J.-Q. Yan, and Y. Ren, *Phys. Rev. Lett.* **99**, 156401 (2007).
- [27] A. Munoz, J. A. Alonso, M. T. Casáis, M. J. Martínez-Lope, J. L. Martínez, and M. T. Fernández-Díaz, *Phys. Rev. B* **68**, 144429 (2003).
- [28] J. Reul, A. A. Nugroho, T. T. M. Palstra, and M. Grüninger, *Phys. Rev. B* **86**, 125128 (2012).
- [29] M. De Raychaudhury, E. Pavarini, and O. K. Andersen, *Phys. Rev. Lett.* **99**, 126402 (2007).
- [30] X.-J. Zhang, E. Koch, and E. Pavarini, *Phys. Rev. B* **105**, 115104 (2022).
- [31] K.I. Kugel and D.I. Khomskii, *Zh. Eksp. Teor. Fiz.* **64**, 1429 (1973) [*Sov. Phys. JETP* **37**, 725 (1973)].
- [32] X.-J. Zhang, E. Koch, and E. Pavarini, *Phys. Rev. B* **106**, 115110 (2022).
- [33] E. Pavarini, E. Koch, A.I. Lichtenstein, *Phys. Rev. Lett.* **101**, 266405 (2008).
- [34] E. Pavarini and E. Koch, *Phys. Rev. Lett.* **104**, 086402 (2010).
- [35] X.-J. Zhang, E. Koch, and E. Pavarini, *Phys. Rev. B* **102**, 035113 (2020).
- [36] J. Musshoff, G. Zhang, E. Koch, E. Pavarini, *Phys. Rev. B* **100**, 045116 (2019).
- [37] C. Autieri, E. Koch, and E. Pavarini, *Phys. Rev. B* **89**, 155109 (2014).
- [38] P. Blaha, K. Schwarz, P. Sorantin, and S. Trickey, *Comput. Phys. Commun.* **59**, 399 (1990).
- [39] N. Marzari and D. Vanderbilt, *Phys. Rev. B* **56**, 12847 (1997).
- [40] A. A. Mostofi, J. R. Yates, Y.-S. Lee, I. Souza, D. Vanderbilt, and N. Marzari, *Comput. Phys. Commun.* **178**, 685 (2008); J. Kuneš, R. Arita, P. Wissgott, A. Toschi, H. Ikeda, and K. Held, *ibid.* **181**, 1888 (2010).
- [41] T. Mizokawa and A. Fujimori, *Phys. Rev. B* **54**, 5368 (1996).
- [42] E. Pavarini, A. Yamasaki, J. Nuss, and O. K. Andersen, *New J. Phys.* **7**, 188 (2005).
- [43] E. Gull, A. J. Millis, A. I. Lichtenstein, A. N. Rubtsov, M. Troyer, and P. Werner, *Rev. Mod. Phys.* **83**, 349 (2011).
- [44] A. Flesch, E. Gorelov, E. Koch, and E. Pavarini, *Phys. Rev. B* **87**, 195141 (2013).
- [45] J. Musshoff, G. R. Zhang, E. Koch, and E. Pavarini, *Phys. Rev. B* **100**, 045116 (2019).
- [46] J. Musshoff, A. Kiani, and E. Pavarini, *Phys. Rev. B* **103**, 075136 (2021).
- [47] Defining V_1 and V_2 two neighboring sites in one layer and V_3 and V_4 the corresponding ones in the layer above, with V_3 on top of V_1 , in the GdFeO_3 -type structure, if $|\theta, \phi\rangle^1$ is the hole orbital at site V_1 , the hole orbitals at the other sites are $|\theta, \phi\rangle^2 = |\theta, \frac{\pi}{2} - \phi\rangle^1$, $|\theta, \phi\rangle^3 = |-\theta, \phi\rangle^1$, and $|\theta, \phi\rangle^4 = |-\theta, \frac{\pi}{2} - \phi\rangle^1$, respectively. In the monoclinic case, the relation $|\theta, \phi\rangle^3 \sim |-\theta - \delta_\theta, \phi \pm \delta_\phi\rangle$ maximizes the energy gain with $\delta_\theta \sim 20^\circ$ and $\delta_\phi \sim 110^\circ$ in the PM phase.
- [48] For additional information see Supplemental Material.
- [49] For a given spin rank q , there are only two independent saturation ($T \rightarrow 0$) values. This is because, for a specific hole orbital, $\langle \hat{\tau}_i^{r,\mu} \rangle_\alpha = \langle \theta, \phi | \hat{\tau}_i^{r,\mu;q\nu} | \theta, \phi \rangle_\alpha$, depend on two variables only, θ and ϕ [48]. These constraints do not hold at finite temperature, however.
- [50] The CF affects T_N more for C-type than G-type magnetic order, making the first more stable.